Molecular dynamics study on evaporation and condensation of *n*-dodecane at liquid–vapor phase equilibria

Bing-Yang Cao,[1,2] Jian-Fei Xie,[2] and Sergei S. Sazhin[2,a)]
[1]*Key Laboratory for Thermal Science and Power Engineering of Ministry of Education, Department of Engineering Mechanics, Tsinghua University, Beijing 100084, People's Republic of China*
[2]*Sir Harry Ricardo Laboratories, School of Computing, Engineering and Mathematics, University of Brighton, Cockcroft Building, Brighton BN2 4GJ, United Kingdom*

(Received 5 October 2010; accepted 28 March 2011; published online 28 April 2011)

Molecular dynamics simulations are performed to study the evaporation and condensation of *n*-dodecane ($C_{12}H_{26}$) at temperatures in the range 400–600 K. A modified optimized potential for liquid simulation model is applied to take into account the Lennard-Jones, bond bending and torsion potentials with the bond length constrained. The equilibrium liquid–vapor *n*-dodecane interface thickness is predicted to be ~1.2–2.0 nm. It is shown that the molecular chains lie preferentially parallel to the interface in the liquid–vapor transition region. The predicted evaporation/condensation coefficient decreased from 0.9 to 0.3 when temperature increased from 400 to 600 K. These values can be used for the formulation of boundary conditions in the kinetic modeling of droplet heating and evaporation processes; they are noticeably different from those predicted by the transition state theory. We also present the typical molecular behaviors in the evaporation and condensation processes. The molecular exchange in condensation, typical for simple molecules, has never been observed for *n*-dodecane molecular chains. © *2011 American Institute of Physics*. [doi:10.1063/1.3579457]

I. INTRODUCTION

The importance of accurate and computer efficient modeling of droplet heating/cooling and evaporation/condensation in various engineering and environmental applications is widely recognized.[1–8] Most of the models of these processes have been based on the hydrodynamic approximation, when vapor in the immediate vicinity of droplet surfaces is assumed to be always saturated, and the problem of droplet evaporation/condensation reduces to the problem of vapor diffusion to/from the ambient gas.[5] In a number of papers, however, it was pointed out that this almost universally acceptable approach can lead to errors of up to about 10% in modeling small droplet heating and evaporation even in dense gases (diesel engine-like conditions).[9–12] In these papers, a new model for droplet heating and evaporation has been developed based on the combination of the kinetic and hydrodynamic approaches. In the immediate vicinity of droplet surfaces (up to about 100 molecular mean free paths), the vapor and ambient gas dynamics were studied based on the Boltzmann equation (kinetic region), while at larger distances the analysis was based on the hydrodynamic equations (hydrodynamic region). Mass, momentum, and energy fluxes were conserved at the interface between these regions. The predictions of this model were shown to be as accurate as those of the model based on the kinetic equation in the whole domain. One of the main drawbacks of this model is that it was based on the assumption that we know the evaporation coefficient of the liquid, which is not true in the case of *n*-dodecane. Hence, crude estimates of this coefficient were used. The need to know the evaporation/condensation coefficient has also been discussed in a number of other kinetic models and molecular dynamics (MD) simulations of interface phenomena.[13–18]

A rigorous theoretical estimation of the evaporation and condensation coefficients requires the application of molecular dynamics methods.[19–27] Perhaps one of the most advanced molecular dynamics investigations of these coefficients for water was reported by Tsuruta and Nagayama.[19] In this paper, two models for intermolecular potential were used: the Carravetta and Clementi model[28] and the extended simple point charge model.[29] In both models, the intermolecular interactions were treated as a combination of the short-range pairwise potential of atoms and the long-range Coulombic interaction. The predictions of the extended simple point charge model were shown to be in better agreement with the experimental data than those of the Carravetta and Clementi model. It was pointed out that translational motion is of primary importance for the evaporation/condensation process, whereas the effects of rotational motion are insignificant.

The molecular dynamic simulation data for argon and water were shown to be in good agreement with the prediction of the evaporation/condensation coefficient by the transition state theory, developed by Penner.[30,31] This theory was further improved by Nagayama and Tsuruta.[32] In the latter paper, condensation/ evaporation processes at the liquid–vapor interface were considered as a kind of chemical reaction and the general theory of rate processes was applied.[33] As a result, the following simple expression for the evaporation/condensation coefficient was derived:

a)Author to whom correspondence should be addressed. Electronic mail: s.sazhin@brighton.ac.uk.

$$\alpha = \left[1 - \left(\frac{V^l}{V^g}\right)^{1/3}\right] \exp\left[-\frac{1}{2}\frac{1}{\left(\frac{V^g}{V^l}\right)^{1/3} - 1}\right], \qquad (1)$$

where V^l and V^g are specific volumes of liquid and gas, respectively. Remembering that $V^l \ll V^g$ for heavy *n*-alkanes, including *n*-dodecane, except when the temperatures are close to the critical temperature, it was assumed that $\alpha = 1$. The transition state theory does not consider detailed structures and motions in chainlike molecules and complex evaporation/condensation behaviors, as discussed in Sec. III D. The application of Eq. (1) to *n*-dodecane needs more rigorous justification, based on molecular dynamics simulations.

A number of models have been developed to describe the dynamics of complex hydrocarbon molecules, such as *n*-dodecane, including the optimized potential for liquid simulation(OPLS), originally suggested by Jorgensen *et al.*,[34] and the de Pablo and Toxvaerd models. These models are reviewed by Smit *et al.*,[35] who also suggested their new model, based on the OPLS model, which was claimed to be more accurate than the ones suggested earlier. All these models are based on the observation that the C–H bond in complex hydrocarbon molecules is much shorter and much stronger than the C–C bond, and also stronger than the van der Waals forces between molecules. Thus the methyl (CH_3) or methylene (CH_2) groups can be regarded as separate atomlike structures in a relatively simple united atom model (cf. Simon *et al.*[36]). The underlying physics of all these models is essentially the same, but they differ by the values of energy parameters ε for CH_3 and CH_2, diameters of these groups, and bond bending and torsion potentials. Smit *et al.*[35] applied all the above mentioned models to complex hydrocarbons to determine their vapor–liquid coexistence curves, using the simulation based on the Gibbs-ensemble technique and the configuration-bias Monte Carlo method. All models gave nearly identical results at standard conditions but predicted critical temperatures, which could differ by up to 100 K (the critical temperature is mainly controlled by the ratio $\varepsilon_{CH_3}/\varepsilon_{CH_2}$). It was claimed that the new model developed by Smit *et al.*[35] gave a good description of the phase behavior of this curve over a large temperature range. Simon *et al.*[36] applied the Toxvaerd model to the molecular dynamic simulation of *n*-octane. Previous molecular dynamics simulations on *n*-alkane liquid-vapour interfaces focused on interfacial properties, such as phase equilibria, interface tension and thermodynamic parameters.[37–41] However, none of these studies focused on the molecular dynamics analysis of the vapor–liquid equilibria of *n*-dodecane (the closest approximation to diesel fuel) and the estimation of the evaporation/condensation coefficient for this substance.

The focus of this paper is on the application of the OPLS model, modified by Smit *et al.*,[35] to the study of the *n*-dodecane ($C_{12}H_{26}$) liquid–vapor interfaces and the estimation of the evaporation/condensation coefficient. In Sec. II, the details for the model and simulation method are introduced. In Sec. III, the model and method are applied to study the interfacial thickness, density profile, chain orientation, evaporation/condensation coefficient, and typical evaporation/condensation behaviors at the *n*-dodecane liquid–vapor interface. The main results of the paper are summarized in Sec. IV.

II. THE MODEL AND SIMULATION

A. Model

Following the original OPLS model, methyl (CH_3) and methylene (CH_2) groups are regarded as united atoms. In these groups, hydrogen atoms are not modeled separately as distinct atoms. Hereafter we refer to united atoms as atoms and molecules as chains. The essence of the united atom model applied to *n*-dodecane is schematically illustrated in Fig. 1.

The nonbonded interactions between atoms, which belong to either different chains or the same chain but which are more than four atoms apart (there should be at least three atoms between the interacting atoms), are characterized by the truncated Lennard-Jones (LJ) potential,

$$u^{LJ}(r_{ij}) = 4\varepsilon_{ij}\left[\left(\frac{\sigma_{ij}}{r_{ij}}\right)^{12} - \left(\frac{\sigma_{ij}}{r_{ij}}\right)^{6}\right]. \qquad (2)$$

The energy parameters of CH_2 and CH_3 groups (atoms) are $\varepsilon_{CH_2}/k_B = 47$ K and $\varepsilon_{CH_3}/k_B = 114$ K, respectively (k_B is the Boltzmann constant). According to the Lorentz–Berthelot rule,[42,43] the energy parameter between CH_2 and CH_3 groups is $(\varepsilon_{CH_2-CH_3})/k_B = \sqrt{\varepsilon_{CH_2}\varepsilon_{CH_3}}/k_B = 73.2$ K. The diameter parameters of the methylene and methyl groups are assumed to be equal and estimated as $\sigma = 3.93 \times 10^{-10}$ m. The LJ interaction is truncated at 13.8×10^{-10} m in our simulations.

The interactions within the chains include bond bending and torsion with the bond length constrained at 1.53×10^{-10} m. These are schematically illustrated in Fig. 2 for the chain portion consisting of four atoms. Bending can take place between any three neighboring atoms. For bond bending between three atoms, as illustrated in Fig. 2, the van der Ploeg

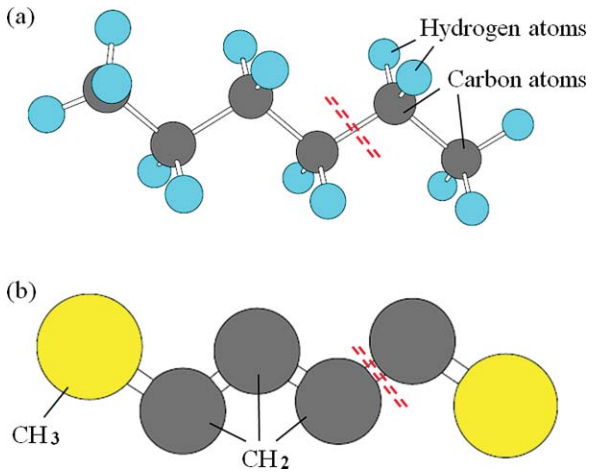

FIG. 1. Schematic presentation of an *n*-dodecane molecule (a) and its presentation using the united atom model (b). The bending angles between neighboring bonds (~114°) (zigzag structure of the molecule) are taken into account.

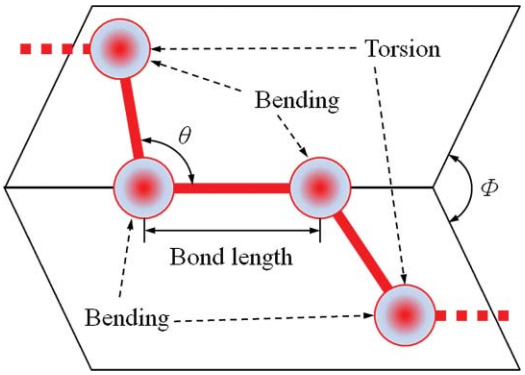

FIG. 2. Schematic presentation of the bonds and the interactions between atoms for a portion of the *n*-dodecane chain, consisting of four united atoms.

and Berendsen potential is used,[44]

$$u^{\text{bend}}(\theta) = \frac{1}{2}k_\theta(\theta - \theta_0)^2, \tag{3}$$

where the bending coefficient is estimated as $k_\theta/k_B = 62500$ K/rad^2, and the equilibrium angle is $\theta_0 = 114^\circ$. Torsion can take place between four neighboring atoms. For the torsion potential between two atoms with two atoms between them (see Fig. 2), the Jorgensen *et al*. torsion potential is applied:[34]

$$u^{\text{tors}}(\text{Ø}) = c_0 + 0.5c_1(1 + \cos \text{Ø}) + 0.5c_2(1 - \cos 2\text{Ø}) + 0.5c_3(1 + \cos 3\text{Ø}), \tag{4}$$

where

$c_0/k_B = 0$ K, $c_1/k_B = 355$ K, $c_2/k_B = -68.19$ K, and $c_3/k_B = 791.3$ K.

B. Simulation

A system of 400 chains (4800 atoms) is considered in a three-dimensional rectangular simulation box of $51.39\sigma \times 13.73\sigma \times 13.73\sigma$, where σ is a rescaled length used in our simulations as specified in Table I, for liquid temperatures 400, 450, 500, 550, and 600 K. This size of box corresponds to 20.19 nm × 5.39 nm × 5.39 nm. The number of molecules was chosen in such a way that their number density was close to that of a liquid at atmospheric pressure. These chains were oriented along the x axis and initially placed in the middle of the simulation box. They had zigzag configurations [see Figs. 1(b) and 2], and the numbers of chains in three directions were 4, 10 and 10, respectively. The accuracy and reliability of the results have been checked by adding the results of calculations for 720 molecules (see Table II and the relevant discussions).

TABLE I. Rescaled physical parameters used in the MD simulations.

Parameters	Rescaled units
Mass (m^*)	$m_{CH_2} = 2.3252 \times 10^{-26}$ kg
Energy (ε^*)	$\varepsilon_{CH_2} = 0.6486 \times 10^{-21}$ J
Length (l^*)	$\sigma = 3.93 \times 10^{-10}$ m
Temperature (T^*)	$\varepsilon_{CH_2}/k_B = 47$ K
Number density (n^*)	$\sigma^{-3} = 1.647 \times 10^{28}$ m^{-3}
Time (t^*)	$\tau = \sigma\sqrt{m/\varepsilon_{CH_2}} = 2.353 \times 10^{-12}$ s
Velocity (v^*)	$\sigma/\tau = 167$ m/s

The equations of motion of the atoms were integrated using the Verlet leapfrog method.[42,43] For *n*-dodecane chains, the bond length constraints refer only to the near-neighbor atoms. Therefore, the bond lengths could be constrained by the SHAKE scheme adjusting the atom coordinates one by one cyclically to satisfy a given tolerance.[42,43,45] The time step in all simulations was taken equal to 0.002τ, which corresponds to 5 fs. Periodic boundary conditions were applied in all directions. For calculation efficiency, rescaled units were used for most physical parameters as indicated by the superscript "*" in Table I (the values of other thermodynamic parameters can be found in Ref. 46).

The system was then relaxed with a constraint of fixed homogeneous temperature. The *n*-dodecane chains started to relocate within the liquid phase and to evaporate gradually. We monitored the system temperature, pressure, density, molecular configuration, and interface locations to determine whether or not the system reached equilibrium. Typically this requires 1500 ps. Finally the liquid film was sandwiched between the layers of the vapor phases [see Fig. 3(b)]. The densities in the liquid and vapor zones gradually approached those of actual liquid and vapor. Then we started sampling data for another 1000 ps. The positions of the two liquid–vapor interfaces were identified by the density profiles. The interface parameters, such as density, orientation, and evaporation/condensation coefficient, were obtained by averaging them over these 1000 ps.

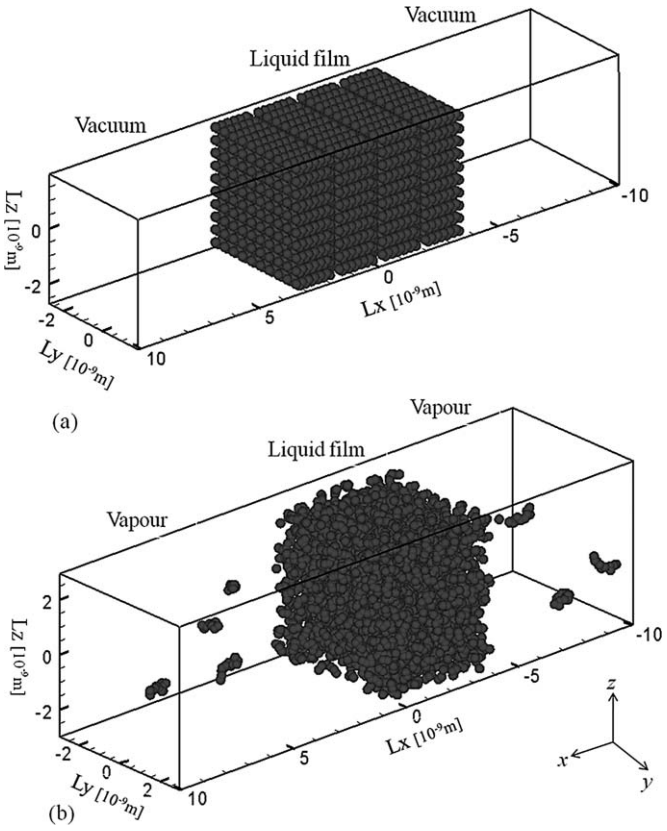

FIG. 3. Snapshots of the simulation system: initial state (a) and liquid–vapor equilibrium (b).

TABLE II. Fractions of various condensation behaviors at $T_l = 500$ K. The values in parentheses in $\langle J_{\rm cond}^{\rm spon}\rangle$, $\left\langle J_{\rm cond}^{\rm trap}\right\rangle$, and $\langle J_{\rm cond}^{\rm refl}\rangle$ columns are the fractions of mass flux of spontaneous, trapping-desorption, and reflection condensations, respectively.

Molecules (Atoms)	$\langle J_{\rm cond}^{\rm spon}\rangle$ [kg/(m^{2}s)]	$\left\langle J_{\rm cond}^{\rm trap}\right\rangle$ [kg/(m^{2}s)]	$\langle J_{\rm cond}^{\rm refl}\rangle$ [kg/(m^{2}s)]	$\langle J_{\rm out}\rangle = \rho_v\sqrt{RT_l/(2\pi)}$ [kg/(m^{2}s)]	α_c
400 (4800)	62.2 (10%)	270 (43.3%)	290.8 (46.7%)	623	0.533
720 (8640)	83 (12.1%)	332 (48.4%)	270 (39.5%)	685	0.605

The chosen number of chains enabled us to perform the molecular dynamics simulations using a standard PC (2.83 GHz CPU, 4 GB RAM work station) over reasonable time (about 1 week per simulation). We appreciate that the limitation of this number makes our results preliminary. They are expected to be confirmed based on simulations involving much larger number of chains for which the application of a supercomputer is essential.

III. RESULTS AND DISCUSSION

A. Interfacial properties

The density profiles at 400, 450, 500, 550, and 600 K are shown in Fig. 4. Based on these profiles, we can identify the liquid region with higher density, the vapor region with lower density and the liquid–vapor interface. As can be seen from this figure, the increase in temperature leads to a decrease in the density of liquid and to an increase in the density of vapor. These trends are more clearly shown in Fig. 5. In the same figure, the results of Monte Carlo simulations[35] and experimental results[47] are presented. As can be seen from this figure, the values of densities predicted by both methods and the ones obtained experimentally are close, which provides additional support for our MD results.

The positions of the liquid–vapor interfaces varied from one simulation to another since the interface profiles fluctuated with time.[26] Despite these fluctuations, the statistical position of the liquid–vapor interface remained stable. The explicit identification of the interface region helped us obtain useful information about the interface. The interface thickness was defined as the thickness over a region where the bulk vapor phase changed to bulk liquid phase [in Fig. 4, it is the thickness over which the density of liquid *n*-dodecane changes from $0.95\rho_l$ to $(\rho_v + 0.01\rho_l)$, where ρ_l and ρ_v are densities of bulk liquid and vapor, respectively,[19]]. The thickness of the interface was about 3–5σ (~1.2–2.0 nm). This thickness is very close to that of the interfaces of simpler molecules, such as argon, methanol, and water, though the present *n*-alkane chains have much larger molecular length.[23–29] We also found that the interface (transition region) is thicker at higher temperatures, which should be taken into account when considering the cases with nonhomogeneous temperatures.

The effects of nonhomogeneous local temperatures have been discussed in Refs. 23 to 29. These effects are linked with the deviation from a thermostatic equilibrium of molecules near the interfaces. The translational and rotational energies of molecules were averaged separately and the results are shown in Fig. 6. As follows from Fig. 6(a), these energies are rather low, about 0.008, and almost equal in the liquid phase, as expected. The translational energies of vapor chains near the interface, however, are generally larger than their rotational energy, although considerable fluctuations of these energies are clearly seen (especially in the case of translational energies). This is consistent with the results reported in the literature and can be related to the fact that vapor in the Knudsen layer adjacent to the liquid–vapor interface is in a nonequilibrium state.[19,48–50] We estimated the Knudsen numbers to be in the range 1–10 for temperatures under consideration. The results similar to those shown in Fig. 6(a)

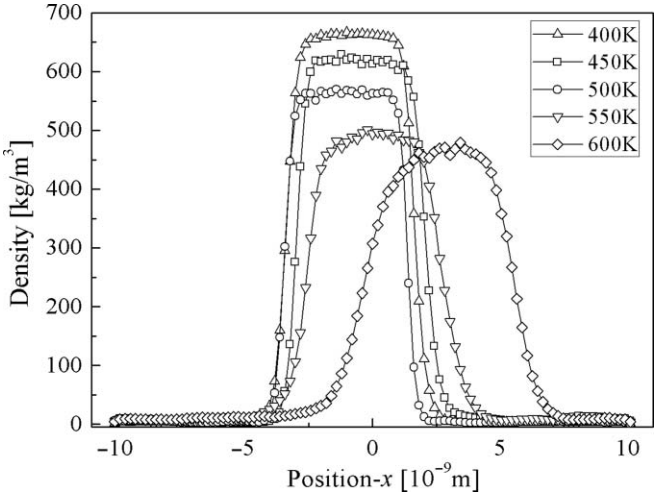

FIG. 4. Density profiles for temperatures 400 K, 450 K, 500 K, 550 K, and 600 K.

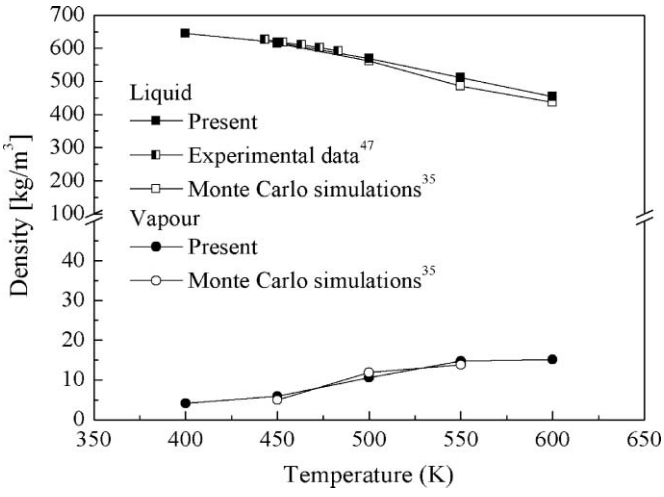

FIG. 5. Liquid and vapor densities vs temperatures for *n*-dodecane at phase equilibria.

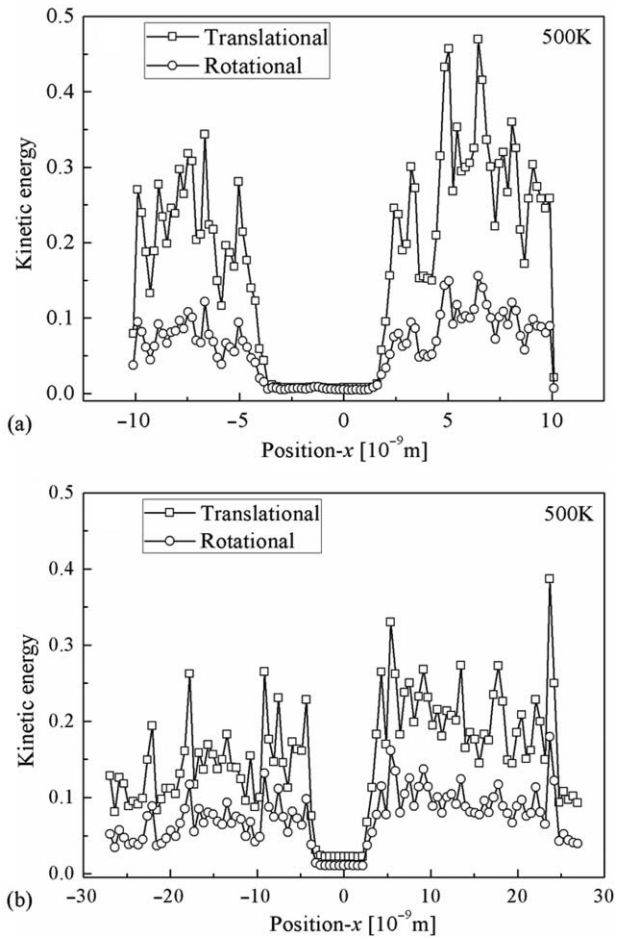

FIG. 6. Local translational and rotational kinetic energies (normalized by ε_{CH_2}; see Table I) of *n*-dodecane molecules vs their positions along the x axis at 500 K for simulation boxes $51.39\sigma \times 13.73\sigma \times 13.73\sigma$ (a) and $137.04\sigma \times 13.73\sigma \times 13.73\sigma$ (b).

but for a larger simulation box are shown in Fig. 6(b). As follows from the latter figure, considerable fluctuations, similar to those shown in Fig. 6(a) are still observed, but there is a clearly recognized trend for translational and rotational energies to approach each other when the distance from the liquid surface increased. This means that the system has a trend of approaching the quasi-equilibrium state in the gas phase away from this surface.

B. Chain orientation at interfaces

The degree of the molecular ordering at the interface was quantified by the orientation order parameter $S(x)$ based on the second order Legendre polynomial,[47]

$$S(x) = \frac{1}{2}\langle 3\sin^2\varphi - 1\rangle, \tag{5}$$

where φ is the angle between the direction of the bonds and the plane perpendicular to the x axis (this plane is parallel to the interface); the averaging was performed over all bonds within a specified slab in the x direction. The range of this parameter is $[-0.5, 1]$. Its positive values indicate the preferential alignment normal to the interface plane (i.e., parallel to the x axis). Negative values indicate the preferential alignment parallel to the interface (i.e., normal to the x axis). Values near 0 show the random alignment. Note that the orientation refers to the backbone of the chains.

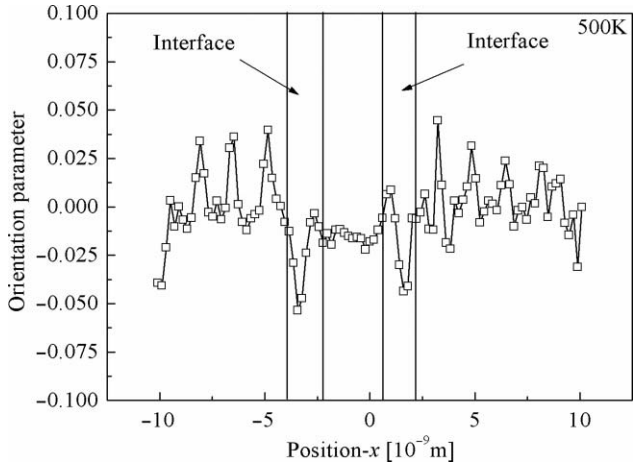

FIG. 7. Local orientation parameter $S(x)$ [see Eq. (5)] of *n*-dodecane molecules vs their positions along the x axis at 500 K.

Typical values of the orientation parameter $S(x)$ at 500 K are shown in Fig. 7. As can be seen from this figure, the chain orientation parameter fluctuates greatly, which implies that the directions of the chains are not completely random in most cases. At the interface region, the orientation parameter tends to be negative (up to -0.05), i.e., the chains lie preferentially [but not completely, which would have been achieved for $S(x) = -0.5$] parallel to the interface, which is consistent with the results obtained for other polymer or *n*-alkane chains.[37,51–53]

This orientation of the chains tends to increase their bonding with the interface, and thus contributes to its stability. Also, this orientation restricts the rotation of molecules in the immediate vicinity of the interface, which is consistent with the earlier mentioned observation that the translation of the chains contributes more to evaporation, than does their rotation.

C. Evaporation/condensation coefficient

The condensation coefficient is defined as the ratio of the condensation flux to the vapor collision flux (the total flux of molecules which hit the liquid surface). As for outgoing evaporation flux, it consists of two components: spontaneous evaporation flux when molecules are emitted from the liquid phase (i.e., the flux not related to the collision flux), and the reflection flux, which is produced by molecules, reflected at the liquid surface. Therefore, the evaporation coefficient is defined as the ratio of the spontaneous evaporation flux to the outgoing evaporation flux. To summarize, the evaporation and condensation coefficients α_c and α_e are defined as[15]

$$\alpha_c = \frac{\langle J_{\rm cond}\rangle}{\langle J_{\rm coll}\rangle}, \quad \alpha_e = \frac{\langle J^{\rm sp}_{\rm evap}\rangle}{(J_{\rm out})}, \tag{6}$$

where $\langle J_{\rm cond}\rangle = \langle J_{\rm coll}\rangle - \langle J_{\rm ref}\rangle$ is the condensation molecular mass flux, $\langle J_{\rm coll}\rangle = -\int v_x f^{\rm coll} dv$ with $v_x < 0$ ($f^{\rm coll}$ is the distribution function of colliding molecules) and $\langle J_{\rm ref}\rangle = -\int v_x f^{\rm ref} dv$ with $v_x > 0$ ($f^{\rm ref}$ is the distribution function

of reflected molecules) are collision and reflection molecular mass fluxes, respectively, $\langle J_{\text{evap}}^{\text{sp}} \rangle$ is the spontaneous evaporation flux, and $\langle J_{\text{out}} \rangle$ is outgoing evaporation flux. Under the equilibrium condition, the condensation flux should be equal to the spontaneous evaporation flux, i.e., $\langle J_{\text{cond}} \rangle = \langle J_{\text{evap}}^{\text{sp}} \rangle$, and the collision flux is also equal to outgoing evaporation flux, i.e.$\langle J_{\text{coll}} \rangle = \langle J_{\text{out}} \rangle$. Thus, we have $\alpha_c = \alpha_e = \alpha$ and define α (hereafter called the evaporation/condensation coefficient) as

$$\alpha = \frac{\langle J_{\text{evap}}^{\text{sp}} \rangle}{\langle J_{\text{out}} \rangle}, \tag{7}$$

[cf. Eq. (1)]. We calculate the spontaneous evaporation flux $J_{\text{evap}}^{\text{sp}}$ by counting the number of molecules crossing unit area per unit time at the interface zone, and $\langle J_{\text{out}} \rangle = \rho_v \sqrt{RT_l/(2\pi)}$ is the outgoing mass flux at the equilibrium state, where ρ_v is saturated vapor density, R is the gas constant, and T_l is the liquid temperature.

The evaporation/condensation coefficient of *n*-dodecane was calculated based on Eq. (7) and our MD simulations for liquid temperatures T_l = 400, 450, 500, 550, and 600 K. The plots of α versus temperature for *n*-dodecane are shown in Fig. 8. As follows from this figure, the evaporation/condensation coefficient, predicted by our analyses, decreases from about 0.9 at 400 K to about 0.3 at 600 K. Similar MD results, reported by various authors for argon, water, and methanol, are shown in the same figure alongside the predictions of the transient state theory [Eq. (1)]. The predictions of transient state theory were based on the densities obtained using our MD simulations. The maximum difference between our results and the predictions of Eq. (1) can be seen at 550 K (69.4%), and the minimum difference at 450 K is 11.4%. Hence, the simulation results do not agree well with the theoretical predictions, based on the transient state theory. Note that in Eq. (7), the maximal possible outgoing molecular mass flux was used and it may result in the underestimation of the evaporation/condensation coefficient at low liquid temperatures due to insufficient molecular mass flux in the vapor phase. Despite this observation, Eq. (7) is still widely used,[10,15,32] and it will be used in our analysis. It is anticipated that the increase in the number of chains used in MD simulations will lead to further increase in the accuracy of our prediction of this coefficient. We completed the simulation in a system with 720 molecules at T_l = 500 K and the results are shown in Table II. As follows from this table, the new value of the condensation coefficient α_c is reasonably close to the prediction of transition state theory, but slightly higher than the one obtained in the case of 400 molecules.

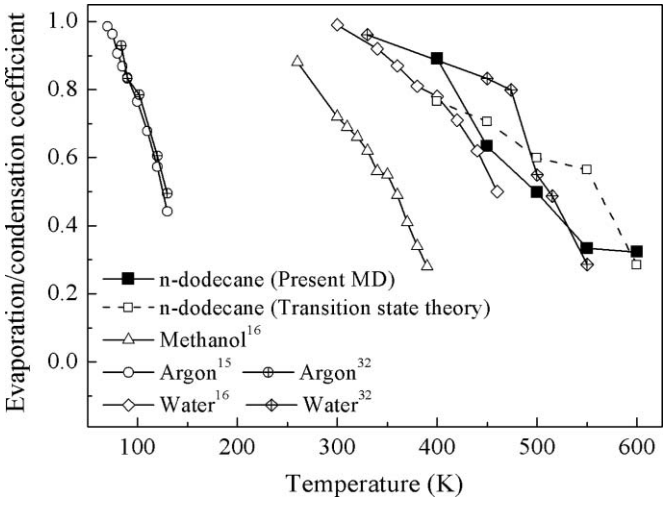

FIG. 8. The values of the evaporation/condensation coefficient for *n*-dodecane vs temperature, as predicted by the present molecular dynamic (MD) simulation and the transition state theory; the values of this coefficient for argon, water, and methanol, obtained by other authors, using MD simulations.

These values of the evaporation/condensation coefficient can be applied to the formulation of the boundary conditions at the *n*-dodecane liquid–vapor interface in the kinetic modeling of droplet heating and evaporation.[9–12] So far the values of this coefficient, used in the modeling, have been assumed equal to those of other substances (e.g., water), or just assumed equal to 1. These crude assumptions obviously undermined the overall accuracy of kinetic modeling.

D. Typical evaporation and condensation behaviors

Several evaporation and condensation behaviors of simple molecules, such as argon, methanol, and water, have been discussed in the literature[15–17,21–26] and are summarized in Fig. 9(a). As follows from our analysis, the behavior of chain molecules can be more complex than shown in this figure; it is schematically presented in Fig. 9(b). The evaporation and condensation behavior of simple molecules normally includes spontaneous evaporation/condensation, reflection evaporation, and molecular exchange, as shown in Fig. 9(a). The behavior of chains includes spontaneous evaporation/condensation [cases 1 and 3 in Fig. 9(b)], reflection evaporation/condensation [cases 2 and 4 in Fig. 9(b)], and trapping-desorption evaporation/condensation [cases 5 and 6 in Fig. 9(b)]. Comparing Figs. 9(a) and 9(b), one can see that cases 1–3 (spontaneous evaporation/condensation and reflective evaporation) are the same for simple and chain molecules. We have not, however, observed any cases of molecular exchange [case 4 in Fig. 9(a)] for chain molecules. This can be related to the fact that, in contrast to simple molecules, chain molecules collide with several molecules in the liquid simultaneously, and the energy transferred to individual molecules appears to be insufficient to remove new molecules from the liquid. To the best of our knowledge, reflection condensation (case 4 in Fig. 9(b)] has never been reported for simple molecules. This can be related to the fact that the collision cross-sections of chain molecules in the interface region are larger, compared with simple molecules. Hence the likelihood of chain molecules leaving the liquid to return to it from the interface region is higher, compared with simple molecules. Note that even for chain molecules, this case is rarely observed. Also, trapping-desorption evaporation/condensation [cases 5 and 6 in Fig. 9(b)] has never been reported for simple molecules to the best of our knowledge. In these cases, the chains can be trapped inside the liquid–vapor interface for a long time and lose memory of their origin: vapor or liquid. Hence, the term trapping-desorption which we suggest for this case.

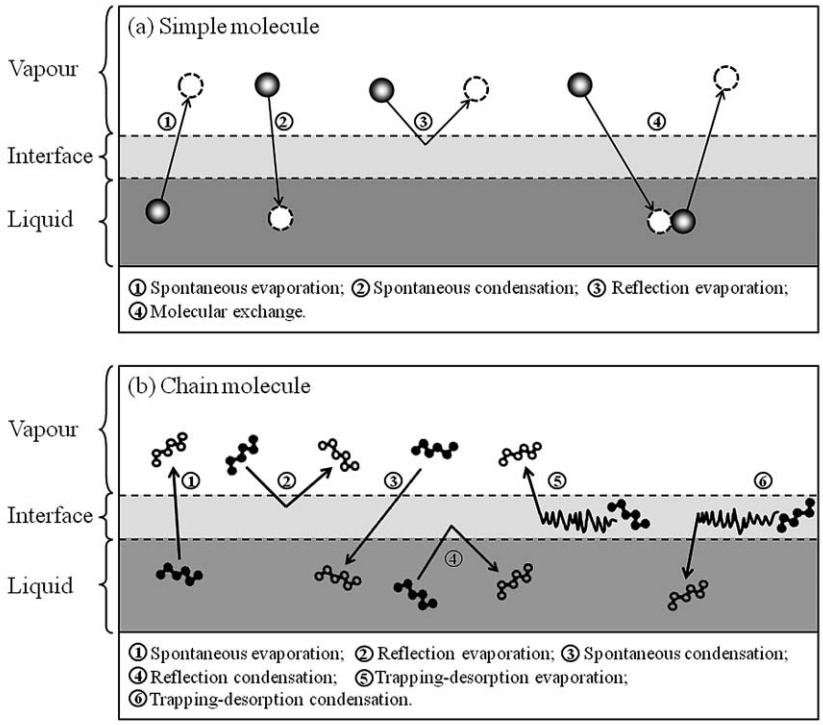

FIG. 9. Schematic presentation of typical evaporation and condensation behaviors of simple molecules (a) and *n*-dodecane chains (b).

All six cases for chain molecules, schematically shown in Fig. 9(b), are illustrated in Fig. 10, based on the analysis of trajectories (positions along x axis) of the centers of mass of individual *n*-dodecane molecules. A classic example of the spontaneous evaporation process [case 1 in Fig. 9(b)] is illustrated in Fig. 10(a). As can be seen in this figure, the trajectory of the molecule inside a liquid is rather complex, but its transit time through the interface is very short. An example of reflection evaporation [case 2 in Fig. 9(b)] is illustrated in Fig. 10(b). As can be seen in this figure, the trajectory of the molecule in the vapor phase is rather complex and it stays for a relatively short time in the interface region [although longer than in the case of spontaneous evaporation, shown in Fig. 10(a)]. The cases of spontaneous and reflection condensations, shown in Figs. 10(c) and 10(d), are almost mirror images of the cases of spontaneous and reflection evaporations shown in Figs. 10(a) and 10(b). For spontaneous condensation, the trajectory of the molecule in the vapor phase is rather complex, but the transition through the interface region is relatively short (although longer than for spontaneous evaporation). With regard to reflection condensation, the trajectory of the molecule is also complex. It leaves the liquid phase and returns to it four times during the period shown in Fig. 10(d). The cases of trapping-desorption evaporation/condensation [cases 5 and 6 in Fig. 9(b)] are illustrated in Fig. 10(e). The main difference between these cases and the ones considered earlier is that the molecules spend much more time in the interface region, compared with the cases shown in Figs. 10(a) to 10(d). During this stay in the interface region, the molecules effectively lose memory regarding their origin (liquid or vapor), as mentioned earlier. The trapping-desorption evaporation process is illustrated on the left-hand side of Fig. 10(e). The evaporated molecule reaches the computational boundary at large positive x. Since the periodic boundary condition was imposed at this boundary, the molecule re-emerges at another periodic boundary at negative x. Eventually, it reaches the interface region, and, after spending considerable time in this region, it re-enters the liquid phase (trapping-desorption condensation).

Note that the above mentioned cases 1–6 in Fig. 10 make different contributions to evaporation and condensation processes. As shown in Table II, for the case of 400 molecules the molecular mass flux of spontaneous condensation $\langle J_{\mathrm{cond}}^{\mathrm{spon}} \rangle$, trapping-desorption condensation $\langle J_{\mathrm{cond}}^{\mathrm{trap}} \rangle$, and reflection condensation $\langle J_{\mathrm{cond}}^{\mathrm{refl}} \rangle$ are 62.2, 270, and 290.8 kg/(m^{2}s), which correspond to 10%, 43.3%, and 46.7%, respectively. This indicates that the trapping-desorption condensation contributes more than does the spontaneous condensation. Also, we can see from the same table that for the system with 720 molecules the same trends are observed. The molecular mass flux of spontaneous condensation, trapping-desorption condensation and reflection condensation are 83, 332, and 270 kg/(m^{2}s), which correspond to 12.1%, 48.4%, and 39.5%, respectively. This trend is attributed to the ordering of the *n*-dodecane molecules inside the liquid–vapor interface. A molecule cannot easily get through a stable array of chain layers. Hence, the molecular behavior should be taken into account when studying the evaporation and condensation of *n*-dodecane, and probably other *n*-alkanes.

Note that there is some ambiguity regarding the physical nature of the "reflection condensation." In fact, we could say that in this case the liquid molecule does not evaporate

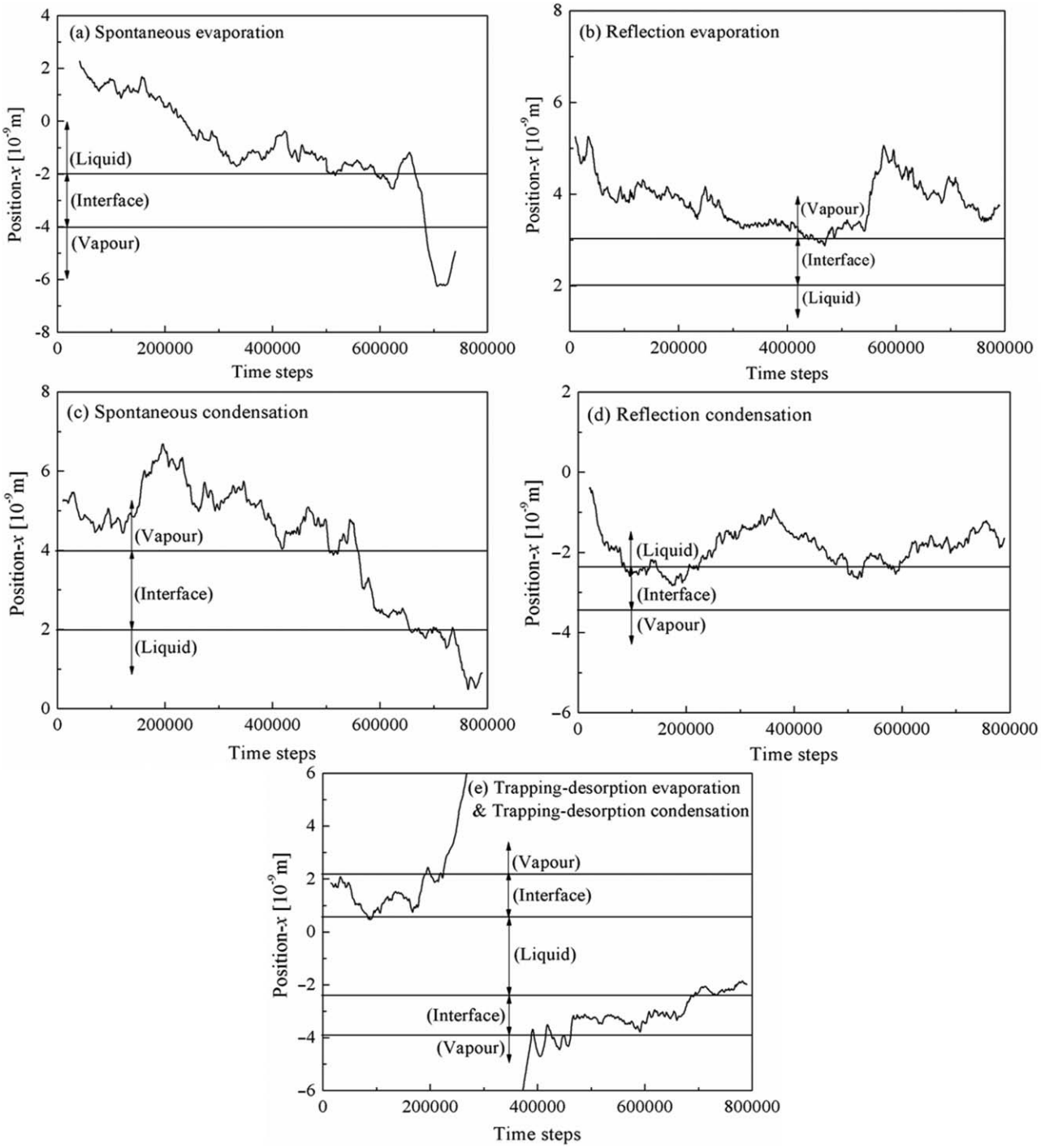

FIG. 10. Typical trajectories of the centers of mass of *n*-dodecane molecules during spontaneous evaporation (a), reflection evaporation (b), spontaneous condensation (c), reflection condensation (d), and trapping-desorption evaporation/condensation (e) [see Fig. 9(b) for an explanation of the meaning of these terms].

and condense. We still refer to it as condensation, keeping in mind the above mentioned comment. The main difference between "trapping-desorption evaporation/condensation" and "spontaneous evaporation/condensation" is the length of time molecule stays in the interface region. We appreciate that it would be difficult, if not impossible at the moment, to take into account reflection condensation and trapping-desorption evaporation/condensation in kinetic modeling and experimental measurements.

IV. CONCLUSION

Evaporation and condensation for *n*-dodecane ($C_{12}H_{26}$) at temperatures 400–600 K have been studied based on molecular dynamics simulation, using 400 molecules. A modified OPLS model, taking into account the Lennard-Jones, bond bending and torsion potentials with the bond length constrained, have been used to simulate the processes at the *n*-dodecane liquid–vapor equilibrium interface. The thickness

of this interface is predicted to be in the range ~1.2–2.0 nm. It is pointed out that the molecular chains lie preferentially parallel to the liquid–vapor interface in the immediate vicinity of this interface. The values of the evaporation/condensation coefficient are predicted to decrease from 0.9 to 0.3 when the temperature increases from 400 to 600 K. These values are shown to be rather different from the values predicted by the transition state theory (although the trends were the same), which justifies the need for the development of the molecular dynamics simulation technique to estimate this coefficient. The values of the evaporation/condensation coefficient, obtained in our analysis, can be potentially used for the formulation of the boundary conditions at the droplet surfaces in the kinetic modeling of droplet heating and evaporation processes. Typical molecular behaviors in the evaporation and condensation processes have been identified. It is pointed out that molecular exchange condensation, typical for simple molecules, has never been observed for *n*-dodecane molecular chains.

ACKNOWLEDGMENTS

The authors are grateful to Engineering and Physical Sciences Research Council (EPSRC) (Grant No. EP/H001603/1) of the United Kingdom, the National Natural Science Foundation of China (Grant No. 50976052), and the Cross-discipline Foundation of the Tsinghua National Laboratory for Information Science and Technology (TNList) for their financial support of this project.

[1] G. M. Faeth, Prog. Energy Combust. Sci. **9**, 1 (1983).
[2] J. B. Heywood, *Internal Combustion Engines Fundamentals* (McGraw-Hill, New York, 1988).
[3] E. E. Michaelides, ASME J. Fluid Eng. **125**, 209 (2003).
[4] U. Fritsching, *Spray Simulation* (Cambridge University Press, Cambridge, England, 2004).
[5] S. S. Sazhin, Prog. Energy Combust. Sci. **32**, 162 (2006).
[6] A. Faghri and Y. Zhang, *Transport Phenomena in Multiphase Systems* (Elsevier, New York, 2006).
[7] E. E. Michaelides, *Particles, Bubbles & Drops* (World Scientific, Singapore, 2006).
[8] S. S. Sazhin, Pollack Periodica **4**, 5 (2009).
[9] A. P. Kryukov, V. Y. Levashov, and S. S. Sazhin, Int. J. Heat Mass Transf. **47**, 2541 (2004).
[10] S. S. Sazhin, I. N. Shishkova, A. P. Kryukov, V. Y. Levashov, and M. R. Heikal, Int. J. Heat Mass Transf. **50**, 2675 (2007).
[11] S. S. Sazhin and I. N. Shishkova, Atomization Sprays **19**, 473 (2009).
[12] S. S. Sazhin, I. N. Shishkova, and M. Heikal, Int. J. Eng. Sys. Model. Simul. **2**, 169 (2010).
[13] Y. Sone and H. Sugimoto, Phys. Fluids A **5**, 1491 (1993).
[14] T. Ytrehus and S. Qstmo, Int. J. Multiphase Flow **22**, 133 (1996).
[15] T. Ishiyama, T. Yano, and S. Fujikawa, Phys. Fluids **16**, 2899 (2004).
[16] T. Ishiyama, T. Yano, and S. Fujikawa, Phys. Fluids **16**, 4713 (2004).
[17] T. Ishiyama, T. Yano, and S. Fujikawa, Phys. Rev. Lett. **95**, 084504 (2005).
[18] S. Hardt and F. Wondra, J. Comput. Phys. **227**, 5871 (2008).
[19] T. Tsuruta and G. Nagayama, J. Phys. Chem. B **108**, 1736 (2004).
[20] S. Maruyama, "Molecular dynamics method for micro/nano systems," in *Handbook of Numerical Heat Transfer*, edited by W. J. Minkowycz, E. M. Sparrow, and J. Y. Murthy (Wiley, New York, 2006).
[21] K. Yasuoka and M. Matsumoto, J. Chem. Phys. **101**, 7904 (1994).
[22] M. Matsumoto and K. Yasuoka, J. Chem. Phys. **101**, 7912 (1994).
[23] M. Matsumoto, K. Yasuoka, and Y. Kataoka, Fluid Phase Equilib. **104**, 431 (1995).
[24] M. Matsumoto, Fluid Phase Equilib. **114**, 307 (1998).
[25] T. Tsuruta, H. Tanaka, and T. Masuoka, Int. J. Mass Heat Transf. **42**, 4107 (1999).
[26] Z. J. Wang, M. Chen, Z. Y. Guo, and C. Yang, Fluid Phase Equilib. **183/184**, 321 (2001).
[27] L. Consolini, S. K. Aggarwal, and S. Murad, Int. J. Heat Mass Transf. **46**, 3179 (2003).
[28] V. Carravetta and E. Clementi, J. Chem. Phys. **81**, 2646 (1984).
[29] H. J. C. Berendsen, J. R. Grigera, and T. P. Straatsma, J. Phys. Chem. **91**, 6269 (1987).
[30] S. S. Penner, J. Phys. Chem. **52**, 949 (1948).
[31] S. S. Penner, J. Phys. Chem. **52**, 1262 (1948).
[32] G. Nagayama and T. Tsuruta, J. Chem. Phys. **118**, 1392 (2003).
[33] G. Gladstone, K. J. Laidler, and H. Eyring, *The Theory of Rate Processes* (McGraw-Hill, New York, 1941).
[34] W. L. Jorgensen, J. D. Madura, and C. J. Swenson, J. Am. Chem. Soc. **106**, 6638 (1984).
[35] B. Smit, S. Karaborni, and J. I. Siepmann, J. Chem. Phys. **102**, 2126 (1995).
[36] J. M. Simon, S. Kjelstrup, D. Bedeaux, and B. Hafskjold, J. Phys. Chem. **108**, 7186 (2004).
[37] J. G. Harris, J. Phys. Chem. **96**, 5077 (1992).
[38] J. M. Simon, D. Bedeaux, S. Kjelstrup, J. Xu, and E. Johannessen, J. Phys. Chem. **110**, 18528 (2006).
[39] C. Ibergay, A. Ghoufi, F. Goujon, P. Ungerer, A. Boutin, B. Rousseau, and P. Malfreyt, Phys. Rev. E **75**, 051602 (2007).
[40] D. Zahn, Chem. Phys. Lett. **467**, 80 (2008).
[41] M. A. Amat and G. C. Rutledge, J. Chem. Phys. **132**, 114704 (2010).
[42] M. P. Allen and D. J. Tildesley, *Computer Simulation of Liquids* (Clarendon, Oxford, 1987).
[43] D. C. Rapaport, *The Art of Molecular Dynamics Simulation* (Cambridge University Press, Cambridge, England, 1995).
[44] P. van der Ploeg and H. J. C. Berendsen, J. Chem. Phys. **76**, 3271 (1982).
[45] J. P. Ryckaert, G. Ciccotti, and H. J. C. Berendsen, J. Comput. Phys. **23**, 327 (1977).
[46] B. Y. Cao, J. Chem. Phys. **129**, 074106 (2008).
[47] J. B. Maxwell, *Data Book on Hydrocarbons: Application to Process Engineering* (Van Nostrand, Princeton, NJ, 1955).
[48] Y. Sone and Y. Onishi, J. Phys. Soc. Jpn. **44**, 1981 (1978).
[49] D. A. Labuntsov and A. P. Krykov, Int. J. Heat Mass Transf. **22**, 989 (1979).
[50] K. Aoki, Y. Sone, and T. Yamada, Phys. Fluids A **2**, 1867 (1990).
[51] M. Tsige and S. S. Patnaik, Chem. Phys. Lett. **457**, 357 (2008).
[52] M. Kawamata and T. Yamamoto, J. Phys. Soc. Jpn. **66**, 2350 (1997).
[53] F. Pierce, M. Tsige, O. Borodin, D. Perahia, and G. S. Grest, J. Chem. Phys. **128**, 214903 (2008).